Inorganic Chemistry

pubs.acs.org/IC

Article

Tuning the Fluorometric Sensing of Phosphate on UiO-66-NH_2(Zr, Ce, Hf) Metal Nodes

Mohamed H. Hassan and Silvana Andreescu*

Cite This: *Inorg. Chem.* 2023, 62, 20970−20979

Read Online

ACCESS | Metrics & More | Article Recommendations | Supporting Information

ABSTRACT: Metal−organic frameworks (MOFs) with intrinsic luminescent properties, modular structure, and tunable electronic properties, provide unique opportunities for designing target-specific molecular sensors by systematically choosing their constituent building blocks. We report a simple one-step MOF-based sensing platform for phosphate (P) detection that combines the luminescent properties of 2-aminoterephthalic acid (ATA) with the affinity of rationally selected nodes in UiO-66-NH_2 to bind with P. This MOF possesses an electron-donating amine group that controls the light-harvesting characteristics of the linkers. Substituting Zr_6 node with Ce_6 or Hf_6 results in a series of isostructural MOFs with distinct optical properties that are nonexistent in the unsubstituted MOF. We have utilized these MOFs to quantitatively measure P, using its ability to bind strongly to metal nodes inhibiting the LMCT process and altering the linker's photon emission. Using this system, detection limits of 4.5, 7.2 and 10.5 μM were obtained for the UiO-66-NH_2(Ce), UiO-66-NH_2, and UiO-66-NH_2(Hf) respectively, adopting a straightforward single step procedure. These results demonstrate that the selection of metal nodes in a series of isostructural MOFs can be used to modulate their electronic properties and create sensing probes possessing the desired characteristics needed for the detection of environmental contaminants.

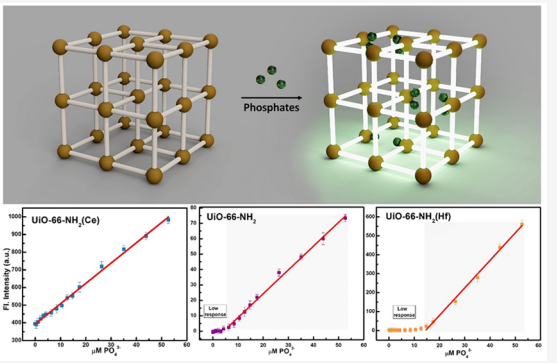

1. INTRODUCTION

Phosphorus is an essential element found in the composition of many biological molecules such as DNA, RNA, ATP, and phospholipid in cell membranes and others.[1] Inorganic phosphates are used in agricultural practices as fertilizers to supply plants with nutrients and increase food production. With the increased use, alarming levels of phosphates have been found in water bodies and agricultural runoff entering lakes and stimulating the growth of harmful algae blooms that spread on water surfaces preventing access of oxygen and sunlight.[2,3] As a result, CO_2 levels increase, forming dead zones leading to deterioration in water quality with many adverse effects on plants and animals.[4] The imbalance in this environment severely affects the photosynthesis and oxygen levels, endangering the sustainability of the aquatic ecosystem.[5]

Conventional and newly discovered materials such as activated carbon, MOFs,[6,7] metal nanoparticles,[8] graphene composites,[9] and others can be used to bind to phosphate (P) and prevent pollution. Identification of zones with high P concentrations that are at risk of eutrophication requires effective tools for monitoring P levels.[10] The conventional analytical test for P detection relies on a tedious and laborious method employing molybdenum blue that involves using a number of reagents and incubation steps, and requires sequential mixing and time monitoring.[11,12] Materials such as MOFs, nanoparticles, metal complexes can be used as potential probes for P but in order to be used for sensing, in addition to P-recognition, they require a transduction modality so that binding can be measured by methods such as fluorometric,[13,14] colorimetric,[15,16] and electrochemical techniques.[17−19] Despite the discovery of many materials with P-binding ability, their use as probes and detection tools that can measure P in eutrophic zones is still limited. In addition, a fundamental understanding of the molecular origin of P recognition and detection capability is still needed to rationally design effective monitoring tools.

The modular nature along with the ability to engineer MOFs with fluorescence capabilities provides a means for MOFs to be used as sensors or probes for detecting target analytes. Replacing the metal node, functionalizing the linker, or doping give rise to products with desired characteristics for specific applications in photocatalysis,[20] sensing,[21] water treatment,[22] and toxic chemicals neutralization.[23,24] UiO-66 is one of the most studied MOFs due to its high chemical stability, tunability, and the rich defect chemistry.[25] Partial or complete metal (M) substitution in the $Zr_6O_4(OH)_4$ node with Ti, Hf,

Received: July 8, 2023
Revised: October 20, 2023
Accepted: October 20, 2023
Published: December 14, 2023

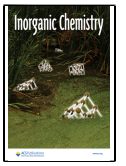

https://doi.org/10.1021/acs.inorgchem.3c02318
Inorg. Chem. 2023, 62, 20970−20979

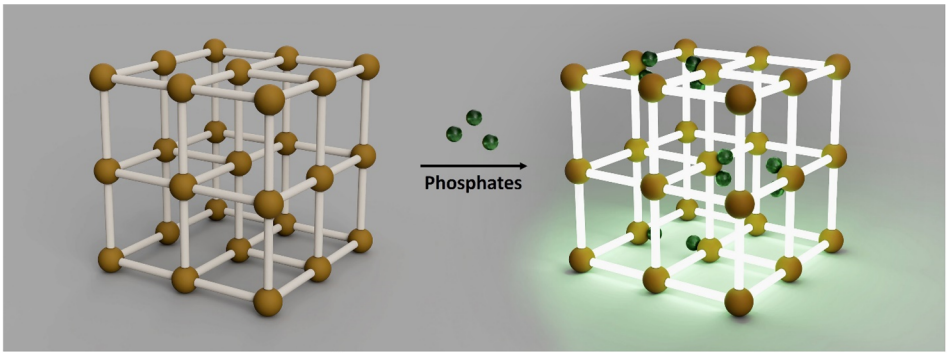

Figure 1. Graphical representation of the phosphate-caused increase in the MOF fluorescence. P is represented as green spheres, while metal clusters are depicted as orange spheres.

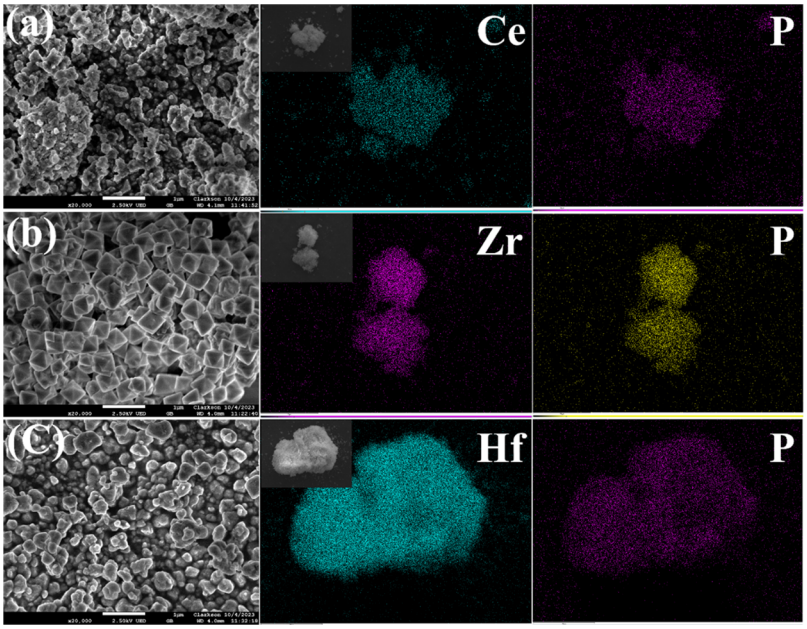

Figure 2. SEM images of (a) UiO-66-NH_2(Ce), (b) UiO-66-NH_2, and (c) UiO-66-NH_2(Hf) and their corresponding elemental mapping.

and Ce and adding functional groups on the link's benzene rings enable modulation of their optical properties. Their luminescence originating from the emitted photons when excited electrons in the singlet state (S_1) return to the ground state (S_0)[26] is particularly useful and amenable to chemical sensing. Changes in luminescence have been utilized in sensing of DNA,[27] temperature,[28] metal ions,[29,30] pH,[31] and others.[32]

Among possible metals that can be used to construct porous frameworks, lanthanides provide electronic configurations giving rise to luminescent properties and affinity towards P that, when combined, show great promise for optical-based chemical sensing.[33] Despite the similar connectivity in Zr, Ce, and Hf-based UiO-66-NH_2, Ce-based MOFs appear to have the highest affinity for P binding, as revealed in several examples demonstrated in the enhanced phosphate ester bond cleavage,[34] DNA hydrolysis,[35] and a superior P removal from eutrophic water.[6] This enhanced performance was ascribed to the possible formation of hybrid orbitals between Ce^{IV} 4f orbitals and P═O bond orbitals.[36] We previously found an enhanced uptake of P from eutrophic water using UiO-66(Ce). Here, we explored the insertion of amine groups on the terephthalic acid (TA) linker to enhance the UiO-66-NH_2(M) fluorescence and studied its interaction with P with the goal of designing a single step fluorescence detection tool, Figure 1. The results provide a mechanistic investigation demonstrating how the use of different metal nodes affects the binding and fluorescence properties when three isostructural MOFs are exposed to P oxyanions. This study enables the rational selection and design of novel sensing probes for rapid one-step detection of P in water environments.

2. RESULTS AND DISCUSSION

The synthesis of UiO-66-NH_2(M) was accomplished by combining Zr^{IV}, Hf^{IV}, and Ce^{IV} metal salts with 2-amino-terephthalic acid (ATA) in DMF or water as the main solvents in the presence of acetic acid as a common modulator. The activated microcrystalline frameworks are characterized by good yields, permanent microporosity, and adequate thermal stability, Figure S2. These isostructural MOFs have twelve-connected octahedral clusters $[M_6O_4(\mu_3\text{-}OH)_4]^{12+}$ bridged ideally by 12 ATA linkers in *fcu* topology. Several studies have reported the coexistence of defect sites in UiO-66 and its analogues in the form of missing linkers and missing clusters.[34,37−39] We utilized acetic acid as a modulator to minimize the variation of synthetic conditions and maintain a nearly similar defect compensation chemistry. Unlike UiO-

https://doi.org/10.1021/acs.inorgchem.3c02318
Inorg. Chem. 2023, 62, 20970−20979

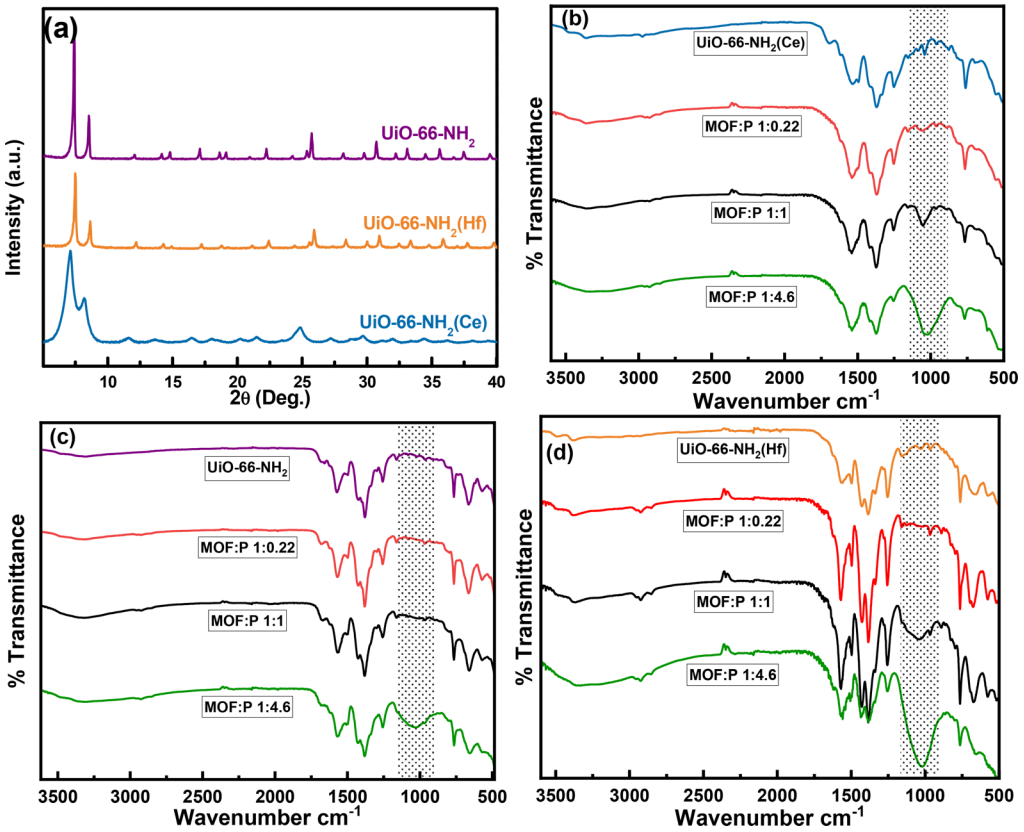

Figure 3. (a) PXRD patterns of UiO-66-NH_2(M). (b) FTIR spectra of UiO-66-NH_2(Ce), (c) UiO-66-NH_2, and (d) UiO-66-NH_2(Hf).

66(M), UiO-66-NH_2(M) could not be obtained using similar synthesis protocol due to the ease of Ce^{IV} reduction during synthesis, especially at high temperatures with redox active linkers (Ce^{III}/Ce^{IV}: 1.61 V vs SHE).[40] Scanning electron microscope (SEM) images of the three MOFs revealed a microcrystalline nature, with UiO-66-NH_2 being more crystalline with distinguishable octahedral crystals (Figure 2a–c). The presence of P was evident in the energy dispersive spectrometry (EDS) mapping after MOF exposure to P and subsequent washing to remove any loosely adsorbed P, as described in the Experimental Section. In addition, EDS spectra display the elemental composition of the three MOFs as shown in Figure S1. The presence of P after successive washing suggests the formation of a strong chemical interaction between P and the MOFs' metal nodes.

PXRD patterns of the three UiO-66-NH_2(M) MOFs indicate their isostructural nature with matching reflections in good agreement with the reported crystal structures (Figure 3a). FTIR spectra of the three MOFs shown in Figure 3b–d are dominated by the linker's vibration bands. The bands that appeared at around 1568 and 1382 cm^{-1} correspond to the ν_{as} (COO^-) and ν_s (COO^-) vibrational modes, respectively. The peak at 1505 nm is related to the C=C ring stretching, while the C–H bending vibration can be seen at 1025 cm^{-1}. A small band appeared at 766 cm^{-1} corresponding to COO^- bending vibration.[41] It is worth mentioning that the calculated values of $\Delta\nu(COO^-) = \nu_{as}(COO^-) - \nu_s(COO^-)$ followed the same trend in the electronegativity for the three metals according to the Pauling and Allen scales. The $\Delta\nu$ values (Zr(193) > Hf(187) > Ce(168)) decrease as the electronegativity decreases from Zr to Ce. This trend is similar to those observed in other M-TA based MOFs.[42] UiO-66-NH_2(M) samples were treated with different concentrations of P corresponding to MOF/P mole ratios of 1:0.22, 1:1 and 1:4.6. These samples were stirred with P solutions for an hour followed by several washing/centrifugation cycles then drying in oven at 80 °C overnight. The highlighted bands that appear around 1000 cm^{-1} in the MOFs' spectra after P treatment are related to P–O vibrations. This clearly indicates the presence of P groups bound within the MOF matrix is not affected even after extensive washing. Interestingly, only UiO-66-NH_2(Ce) showed a P signature at low concentrations, which is expected to result in a lower detection limit and improved selectivity, as discussed later.

It was previously demonstrated that defect sites in UiO-66(M) MOFs are responsible for their improved catalytic activity.[34,43−45] The charges on these sites arise from missing linkers and are neutralized by compensating labile ligands. The nature of these compensating species at the defect sites present in the UiO-66 family depends on the synthetic approach.[37] Terminating species such as formate from DMF decomposition,[38] − OH/-OH_2,[46,47] monocarboxylic modulator,[48] and chlorides[49] were all reported as labile ligands saturating these sites, as estimated by potentiometric acid–base titration, NMR, and TGA analysis.[50,51]

Spectroscopy Measurements. Some UiO-66 MOFs with functionalized ligands are capable of harvesting light, which provides opportunities to study the change of the linker's chemical environment upon interaction with guest molecules via fluorescence measurements. ATA with an amine functionality is special and effective in light-harvesting as the addition of NH_2 group shifts the light absorption of TA to the visible region. When UiO-66-NH_2 is irradiated with light, ligand–metal charge transfer (LMCT) occurs though the transfer of

https://doi.org/10.1021/acs.inorgchem.3c02318
Inorg. Chem. 2023, 62, 20970−20979

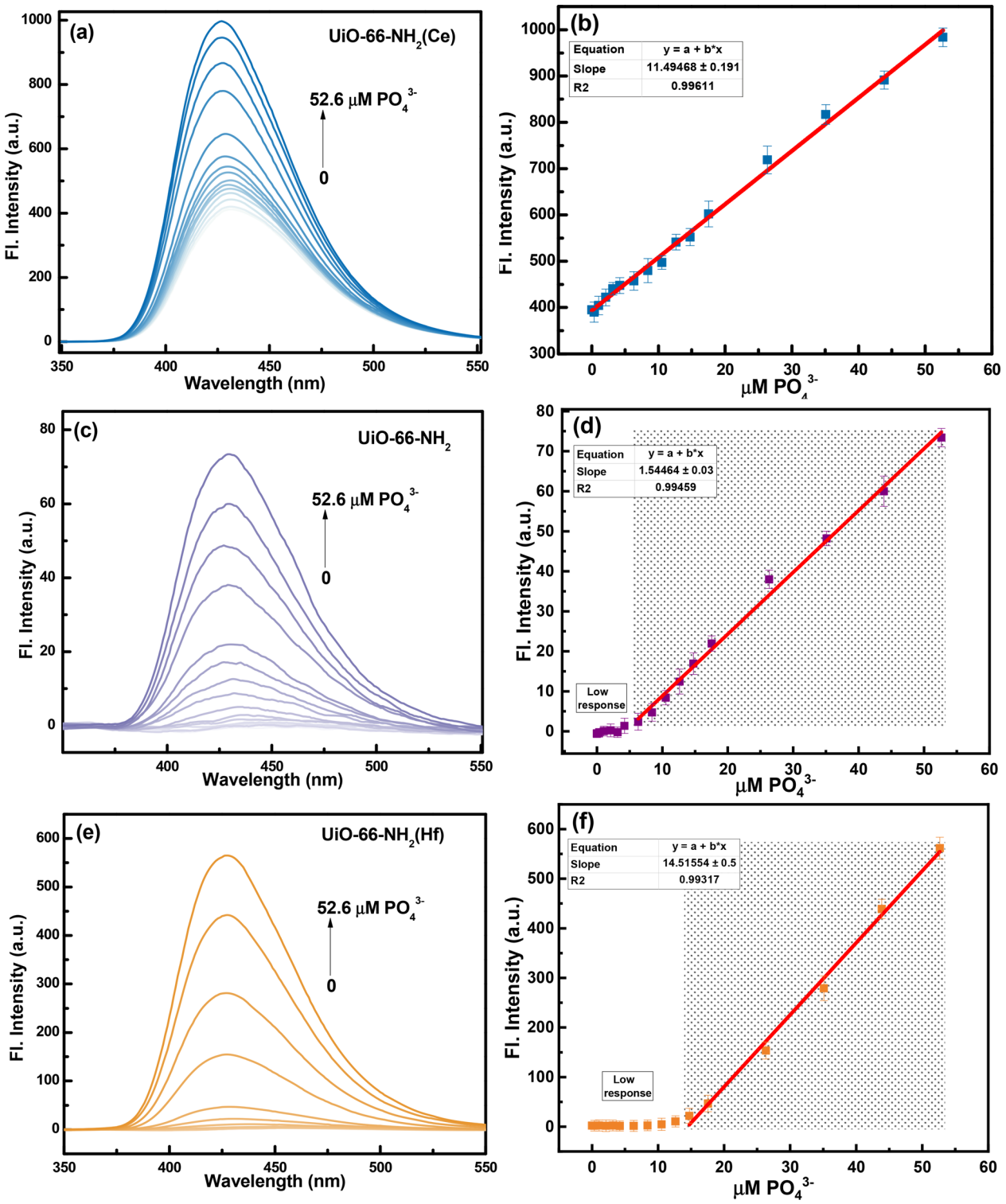

Figure 4. Fluorescence emission spectra (a, c, e) and calibration curves (b, d, and f) of UiO-66-NH_2(Ce), UiO-66-NH_2, and UiO-66-NH_2(Hf) when excited at 328 nm, respectively.

excited electrons from the ATA linker to the Zr^{IV}-oxo cluster reducing Zr^{IV} to Zr^{III} as evidenced by EPR spectroscopy.[52] However, the detected amount of Zr^{III} is very low and dependent on the solvent and temperature.[53]

The charge transfer in this system and in the UiO-66-NH_2(Hf) is suboptimal due to the high energy of their d orbitals rendering their highest occupied (HOCO) and lowest unoccupied (LUCO) crystal orbitals transitions to be ligand-based.[54] On the contrary, the low lying 4f empty orbital of Ce^{IV} and the ease of Ce^{IV} reduction render the LMCT energetically favorable, where these 4f orbitals work as electron trap. The presence of amine groups in UiO-66-NH_2(Ce) made the LMCT more negative (favorable).[55] Upon the addition of increasing concentrations of P to all three MOFs, a turn-on fluorescence signal appeared at 430 nm and increased gradually with P concentration (Figure 4a–f). Additionally, this signal is

https://doi.org/10.1021/acs.inorgchem.3c02318
Inorg. Chem. 2023, 62, 20970−20979

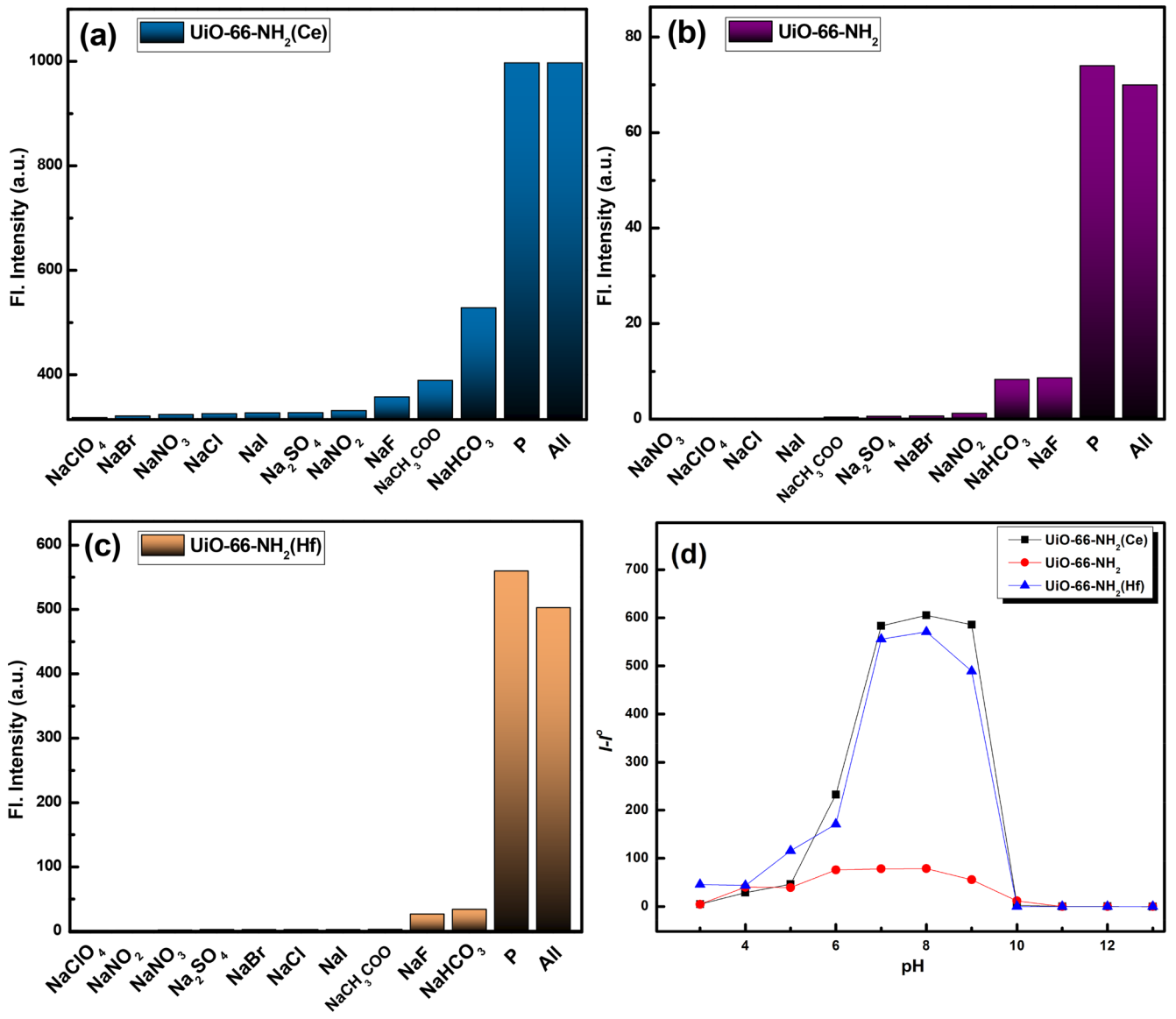

Figure 5. Fluorescence signals at 430nm after the addition of 50 μM of interfering ions to (a) UiO-66-NH_2(Ce), (b) UiO-66-NH_2, and (c) UiO-66-NH_2(Hf). (d) pH on the MOFs' emission intensity.

slightly blue-shifted with the addition of higher concentrations of P, which is probably due to the breakage of M-O bond.

In addition to having an isostructural nature, all three UiO-66-NH_2(M) showed noticeable fluorescence responses in the presence of P in solution. Although all MOFs responded to the presence of P and demonstrated turn-on fluorescence signals at around 430 nm, they showed different sensitivity, selectivity, and detection limits. At low P concentrations, Zr and Hf MOFs showed limited response even after an extended 1 h incubation time. After reaching a threshold concentration, the fluorescence response became more pronounced, and the signal at 430 nm became more visible (Figure 4d,f). UiO-66-NH_2(Ce) showed higher sensitivity to low concentrations of P with no "low response" areas when the experiment was run under similar conditions (Figure 4b). From the linear regions in the calibration curves, the calculated LOD are 4.5, 7.2, and 10.5 μM for UiO-66-NH_2(Ce), UiO-66-NH_2, and UiO-66-NH_2(Hf), respectively.

The effect of several species that exist and are known to interfere with the fluorescence signal was further investigated to quantify the accuracy of the method. Monovalent and divalent anions and oxyanions were added to MOF solutions, and the fluorescence was measured and compared, Figure 5a–c. As seen in the bar graphs, P makes the major contribution to the fluorescence turn-on in all the MOF solutions. Fluoride, carbonate, and acetate have significantly smaller effects on the MOFs' fluorescence, while other species tested ($NaClO_4$, NaBr, NaCl, NaI, Na_2SO_4, $NaNO_2$, and $NaNO_3$) did not cause any noticeable change in the emission. In these experiments, the effect of these ions was measured separately, while they all might be present in P contaminated areas to a certain degree. For this reason, an additional experiment was performed where we combined all the interfering species with P and exposed them to the MOF solutions. In the case of UiO-66-NH_2(Ce), the combined solution causes the MOF to generate a fluorescence signal with the same intensity as that generated by P only. This observation could be explained by a higher affinity of the Ce^{IV}-oxo cluster to bind with P. The same effect was noticed in UiO-66-NH_2 and UiO-66-NH_2(Hf) to some extent, with a slight decrease in the intensity of the signal

https://doi.org/10.1021/acs.inorgchem.3c02318
Inorg. Chem. 2023, 62, 20970−20979

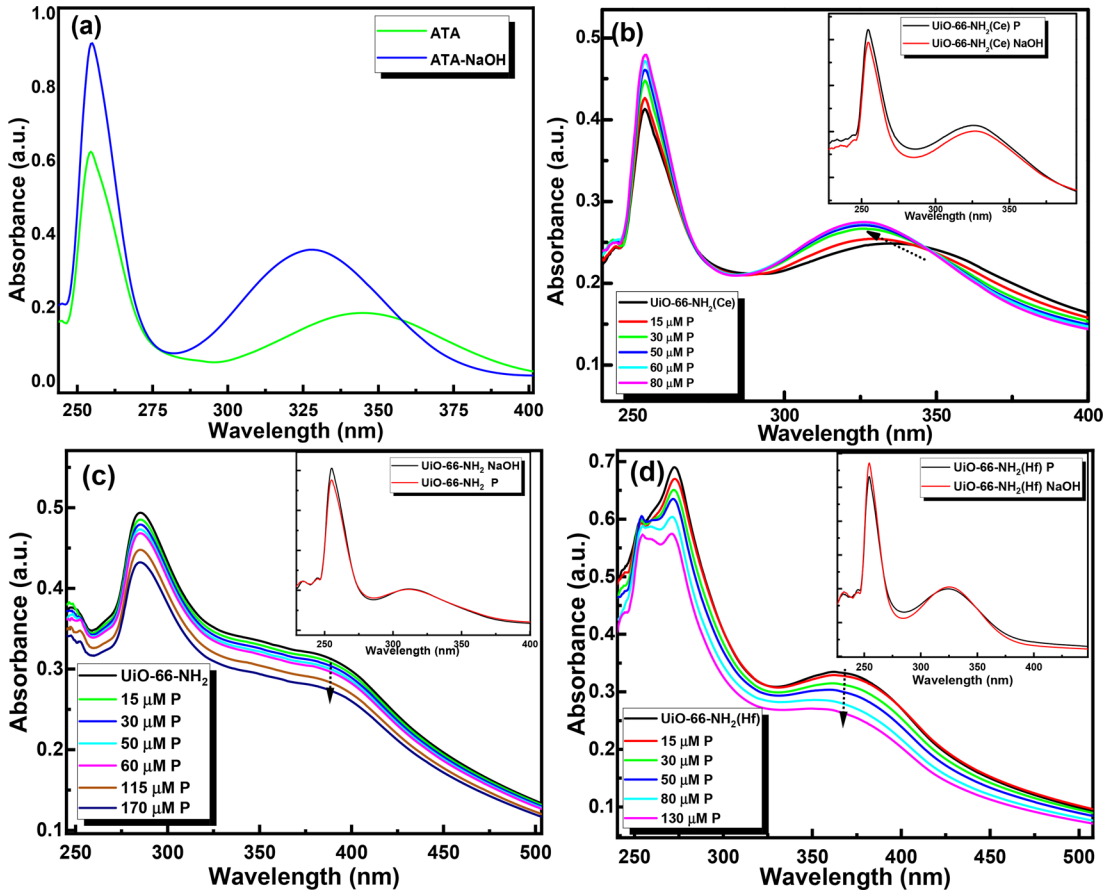

Figure 6. UV−vis spectra of (a) ATA, (b) UiO-66-NH_2(Ce), (c) UiO-66-NH_2, and (d) UiO-66-NH_2(Hf) before and after the addition of NaOH and P.

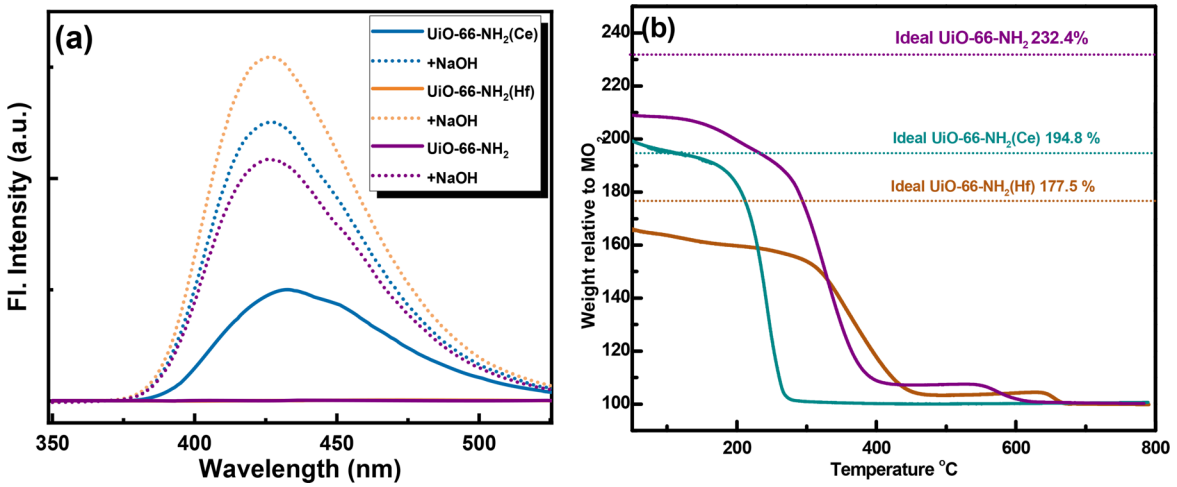

Figure 7. (a) Emission spectra of UiO-66-NH_2(M) after the addition of NaOH, and (b) TGA curves of the MOFs in air.

generated by the combined solutions, as compared to the addition of P only to these MOFs. The effect of the solution pH on the emission intensity before and after P addition was also demonstrated in Figure 5d, showing an obvious dependence on the pH of the environment. At low pH values, the response of the three MOFs to P is low due to the possible protonation of phosphates. At high pH values, these MOFs have high fluorescence before the addition of P. This behavior was expected as hydroxyl ions cause the perturbation of metal−linker bonds, leading to linker release and a strong emission, as discussed in the following section.

To understand the effect of P on the turn-on fluorescence signal, UV/Vis spectra of the MOFs were recorded before and after exposure to P and NaOH (Figure 6a−d). The UiO-66 family is known to be less stable at high pH leading to a complete structural collapse.[56] The strong affinity between high-valence metal ions and hydroxyl anions leads to the collapse of the frameworks though the replacement of the linkers by OH^-.[57] The ATA spectrum shows two absorbance

https://doi.org/10.1021/acs.inorgchem.3c02318
Inorg. Chem. 2023, 62, 20970−20979

peaks at 255 and 345 nm originating from the aromatic ring's sp^2 bonds and the amine functionality, respectively (Figure 6a).[58] The 345 nm peak that appeared due to the interaction of the nitrogen's lone pair with the π^*-orbital of the ring is blue-shifted to 325 nm after the addition of NaOH, which is expected due to the increased dissolution and deprotonation of the ATA causing a shift and increase in the signal.[59] The effect of benzoic acid deprotonation on its absorption spectra was previously shown to cause a blue-shift after the formation of benzoate anions in water, supporting the current findings.[60] Introducing NaOH to UiO-66-NH_2(M) leads to MOF destruction and the release of deprotonated ATA as evidenced by the disappearance of the MOF absorbance peaks and the appearance of the ATA ones. Introducing various (low) concentrations of P to each of the MOF solutions leads to a constant change in the MOF absorbance maxima, indicating a possible alteration in the ligand connectivity (Figure 6b–d). Upon adding a very high concentration of P, the spectra of all the three isostructural MOFs became similar to that of the unprotonated ATA, indicating the attack of P on the SBU and the release of high amounts of ATA in solution.

Monitoring the MOFs' fluorescence after the addition of NaOH gave similar results, as shown in Figure 7a. The addition of NaOH to the MOFs has the same turn-on effect as that of P via enhancing the emission at 430 nm due to the perturbation of M-ATA bonding.

In order to investigate the reason for the presence of low response areas, the infrared spectra of the MOF samples with P concentration in the low regions were inspected, as shown in Figure 3. The mole ratio used in preparing the samples with spectra labeled as 1:0.22 MOF/P corresponds to a concentration of 3.15 μM P in the calibration curve that lies within the low response region. The P–O vibration peak at 1000 cm^{-1} is distinguishable only in the spectrum of UiO-66-NH_2(Ce) at this low concentration but not detectable in the spectra of the other MOFs. Acetic acid is not expected to play a major role in this optical response as it has been shown to leach out upon suspending UiO-66 in water, where water molecules substitute acetate anions.[61] Whether this substitution is partial or full (depending on the pH), it gives an idea of how labile acetates are at the surface of the secondary building units (SBUs). This substitution would leave active sites ready for P binding, enhancing detection sensitivity and enabling sensing of P at low concentrations. Despite the similar physical properties of Ce, Zr, and Hf as they belong to group IV elements, their M–O bond strength is different.[44] Ce forms a slightly weaker bonding with carboxylates compared to Zr and Hf, which has been demonstrated by the decreased mechanical stability of UiO-66(Hf)>UiO-66 > UiO-66-Ce.[62] In our system, thermogravimetric analysis (TGA) of the MOFs revealed that the stability followed the previously mentioned trend (Figure 7b). Moreover, by monitoring the defect density of the MOFs from the TGA curves, UiO-66-NH_2(Ce) has almost no defects unlike UiO-66-NH_2 and UiO-66-NH_2(Hf). The latter two MOFs have about 1.5 missing linkers per cluster, as shown in Figure S3. The complicated synthesis of UiO-66-NH_2(Ce) due to the ease of Ce^{IV} reduction with ATA made it challenging to control its defect density. Based on these observations, the low response areas might be due to the higher stability of UiO-66-NH_2 and UiO-66-NH_2(Hf) that resist the substitution of ATA with P to a certain extent, unlike UiO-66-NH_2(Ce). Moreover, upon addition of P to the MOFs, P first binds to the defect sites and then replaces the linkers at higher concentrations.[63] Since UiO-66-NH_2 and UiO-66-NH_2(Hf) have defect sites, P binds first at these sites, causing no change to the MOFs' fluorescence. After these sites are saturated with P, the excess P leads to metal–ATA bonds dissociation and enhancement of the ATA fluorescence. The lack of defects in UiO-66-NH_2(Ce) might contribute to the higher sensitivity to low P concentrations.

To test the practicality of this method for detecting P in real samples, water from the Delaware river was tested. The water samples were filtered through a syringe filter to remove most of the particulate matter. Samples were spiked with P to reach a final concentration of 40 μM then tested with UiO-66-NH_2(Ce). The water pH was about 7.8, and the emission intensities were converted to P concentrations and are compared in Figure S4. As shown, the calculated concentrations were slightly higher than the added concentration due to the possibility of the presence of small amounts of organic matter, or other unknown interfering species that might increase the fluorescence intensity.

3. CONCLUSION

In summary, we have demonstrated the use of three isostructural UiO-66-NH_2 metal–organic frameworks constructed from group (IV) metal ions as fluorescent probes for the detection of phosphate oxyanions in solution. Despite their structural similarity, UiO-66-NH_2(Ce) showed better sensing performance with a lower limit of detection of 4.5 μM for Ce-UiO-66-NH_2(Ce) as compared to 7.2 and 10.5 μM for UiO-66-NH_2 and UiO-66-NH_2(Hf), respectively. Additionally, this MOF revealed a higher binding affinity and selectivity for P in the presence of interfering species, such as SO_4^{2-}, CH_3COO^-, ClO_4^-, F^-, Cl^-, Br^-, I^-, NO_2^-, NO_3^-, and HCO_3^-. The fluorescence enhancement is ascribed to the perturbation of the linker-metal bonds caused by the binding of P to the metal nodes. This study provides mechanistic information demonstrating that highly porous materials can be used as probes for detection of P upon functionalization of their linkers to impart fluorescence properties. By changing the metal cluster in the MOFs, different sensitivity and selectivity toward P were obtained reflecting the importance of the careful selection of the MOF components and their impact on sensing performance. Further studies are recommended to involve the investigation of fluorescence lifetime measurements, and implementing the new materials in field deployable devices to improve field monitoring of P levels for the benefit of environmental and agricultural communities.

4. EXPERIMENTAL SECTION

All chemicals were purchased from commercial vendors and used as received. Ammonium cerium nitrate (98.5%), 2-aminoterephthalic acid (ATA) (98%), sodium phosphate (96%), and dimethylformamide (DMF) were purchased from Sigma-Aldrich. Hafnium ((IV) chloride (99.9%) was purchased from ThermoFisher, and zirconium (IV) chloride anhydrous (%98) was obtained from Spectrum.

UiO-66-NH_2 was prepared by dissolving $ZrCl_4$ (2.744 mmol) in 80 mL of DMF, ATA (2.744 mmol) in 80 mL of DMF and 200 mol equiv of acetic acid. Mix all solutions after fully dissolving the components by sonication for 20 min. Place the sealed bottle in oven at 120 °C for 24 h. The precipitate was collected by centrifugation and washed several times with DMF and ethanol then dried under vacuum at 120 °C overnight giving a 728 mg UiO-66-NH_2.[64]

UiO-66-NH_2(Hf) was synthesized by dispersing ATA (5 mmol) and $HfCl_4$ (5.2 mmol) in 50 mL of solution of water/acetic acid (30:20, v/v) then refluxed for 20 h. The precipitate was filtered and

https://doi.org/10.1021/acs.inorgchem.3c02318
Inorg. Chem. 2023, 62, 20970–20979

soaked in anhydrous methanol for 3 days, which was replaced by fresh methanol every day. The product is collected and dried under vacuum at 120 °C for 24 h yielding a 1865 mg UiO-66-NH_2(Hf).[65]

UiO-66-NH_2(Ce) was prepared by dissolving 1.5 mmol of ammonium cerium nitrate in 11 mL of acetic acid/H_2O (3:8). Ethanol (20 mL) was added to the previous solution followed by adding 1.5 mmol of ATA while stirring at room temperature for 2 h. The precipitate was collected by filtration and washed with water and ethanol (three times each) and dried under vacuum at 80 °C overnight yielding a 122 mg UiO-66-NH_2(Ce).[66]

Fluorescence measurements. Aqueous suspensions of UiO-66-NH_2(M) were prepared by dispersing 1.25 mg of MOF powder in 50 mL of water under sonication for 5 min. Different concentrations of P (30 μL) were separately added to 3 mL MOF solutions and incubated for 60 min at room temperature. The fluorescence spectra were measured with a 328 nm excitation wavelength and the calibration curves were constructed by plotting the maximum emission intensities at 430 nm. To test the interferences effect, 4.243 μL from 35.35 mM stock solutions of interfering ions were separately added to 3 mL of UiO-66-NH_2(M) solutions and incubated for 60 min. Additionally, all interfering ions and P were combined and added to a separate MOF solution to examine their effect on P induced emission. The intensities of the emission peaks at 430 nm were compared for all interfering species tested under the same conditions. The limits of detection (LOD) were calculated from LOD = $3.3\sigma/S$, where σ is the standard deviation and S is the slope of the calibration curve.

UV−Vis Measurements. 2 mL aliquots from UiO-66-NH_2(M) solutions were placed in cuvettes to which various concentrations of P and NaOH solutions were added.

Materials Characterization. The powder X-ray diffraction (PXRD) measurements were performed on a Malvern PANalytical X'Pert PRO MRD diffractometer using a Si crystal zero background holder. ThermoScientific Nicolet iS-10 was used to record the Infrared absorption spectra (520−4000 cm^{-1} region). Thermogravimetric analysis (TGA, TA Q50) was used to assess the thermal stability of the MOFs until 800 °C and heating rate of 10 °C/min. Fluorescence spectra were recorded on Cary Eclipse spectrophotometer from Agilent. UV−vis spectra were recorded on Agilent 8453 spectrophotometer. Microscope images were recorded with JEOL JSM 7900FLV FE-SEM under 500V bias in Gentle Beam (GB) Mode. Energy Dispersive Spectra were recorded using Oxford Instruments AZtec 65 mm EDS Detector with the AZtec Software Package. Samples were prepared by mixing MOF solutions with 4.6 equivalent P for an hour then washed several times with water and dried at 80 °C overnight. Nitrogen adsorption and desorption isotherms were recorded on a Quantachrome Autosorb IQ automated gas sorption instrument at 77 K using nitrogen gas (Airgas, 99.999%).

■ ASSOCIATED CONTENT

Supporting Information

The Supporting Information is available free of charge at https://pubs.acs.org/doi/10.1021/acs.inorgchem.3c02318.

EDX spectra, N_2 sorption isotherms, TGA, and real sample analysis (PDF)

■ AUTHOR INFORMATION

Corresponding Author

Silvana Andreescu − *Department of Chemistry and Biomolecular Science, Clarkson University, Potsdam, New York 13699, United States;* orcid.org/0000-0003-3382-7939; Email: eandrees@clarkson.edu

Author

Mohamed H. Hassan − *Department of Chemistry and Biomolecular Science, Clarkson University, Potsdam, New York 13699, United States;* orcid.org/0000-0001-7960-1893

Complete contact information is available at: https://pubs.acs.org/10.1021/acs.inorgchem.3c02318

Notes

The authors declare no competing financial interest.

■ ACKNOWLEDGMENTS

This work was supported by grants NSF-2141017, USDA 2023-67021-39750, and by the NYS Center of Excellence in Healthy Water Solutions at Clarkson University. The authors gratefully acknowledge the Karel Czanderna '77 and Dan Shirkey '80 Clarkson Ignite for the graduate fellowship. Any opinions, findings, and conclusions or recommendations expressed in this material are those of the author(s) and do not necessarily reflect the views of the National Science Foundation or the United States Department of Agriculture (USDA).

■ REFERENCES

(1) Walton, C. R.; Ewens, S.; Coates, J. D.; Blake, R. E.; Planavsky, N. J.; Reinhard, C.; Ju, P.; Hao, J.; Pasek, M. A. Phosphorus availability on the early Earth and the impacts of life. *Nature Geoscience* **2023**, *16* (5), 399−409.

(2) Maúre, E. d. R.; Terauchi, G.; Ishizaka, J.; Clinton, N.; DeWitt, M. Globally consistent assessment of coastal eutrophication. *Nat. Commun.* **2021**, *12* (1), No. 6142.

(3) Peyman, N.; Tavakoly Sany, S. B.; Tajfard, M.; Hashim, R.; Rezayi, M.; Karlen, D. J. The status and characteristics of eutrophication in tropical coastal water. *Environmental Science: Processes & Impacts* **2017**, *19* (8), 1086−1103.

(4) Diaz, R. J.; Rosenberg, R. Spreading Dead Zones and Consequences for Marine Ecosystems. *Science* **2008**, *321* (5891), 926−929.

(5) O'Hare, M. T.; Baattrup-Pedersen, A.; Baumgarte, I.; Freeman, A.; Gunn, I. D. M.; Lázár, A. N.; Sinclair, R.; Wade, A. J.; Bowes, M. J. Responses of Aquatic Plants to Eutrophication in Rivers: A Revised Conceptual Model. *Front. Plant Sci.* **2018**, *9*, 451.

(6) Hassan, M. H.; Stanton, R.; Secora, J.; Trivedi, D. J.; Andreescu, S. Ultrafast Removal of Phosphate from Eutrophic Waters Using a Cerium-Based Metal−Organic Framework. *ACS Applied Materials & Interfaces* **2020**, *12* (47), 52788−52796.

(7) Moumen, E.; Bazzi, L.; El Hankari, S. Metal-organic frameworks and their composites for the adsorption and sensing of phosphate. *Coord. Chem. Rev.* **2022**, *455*, No. 214376.

(8) Zhang, L.; Dan, H.; Bukasa, O. T.; Song, L.; Liu, Y.; Wang, L.; Li, J. Low-Cost Efficient Magnetic Adsorbent for Phosphorus Removal from Water. *ACS Omega* **2020**, *5* (39), 25326−25333.

(9) Verma, S.; Nadagouda, M. N. Graphene-Based Composites for Phosphate Removal. *ACS Omega* **2021**, *6* (6), 4119−4125.

(10) Neverova-Dziopak, E.; Kowalewski, Z.; Preisner, M. The universal trophic index: new methodological approach to eutrophication monitoring and control. *Aquat Sci* **2023**, *85* (1), 6.

(11) Franson, M. A. H.; Eaton, A. D.; Clesceri, L. S.; Greenberg, A. E., Eds. *Standard Methods for the Examination of Water and Wastewater*, 18th ed.; American Public Health Association, 1992.

(12) Nagul, E. A.; McKelvie, I. D.; Worsfold, P.; Kolev, S. D. The molybdenum blue reaction for the determination of orthophosphate revisited: Opening the black box. *Analytica chimica acta* **2015**, *890*, 60−82.

(13) Ma, Y.; Zhang, Y.; Li, X.; Yang, P.; Yue, J.-Y.; Jiang, Y.; Tang, B. Linker-Eliminated Nano Metal−Organic Framework Fluorescent Probe for Highly Selective and Sensitive Phosphate Ratiometric Detection in Water and Body Fluids. *Anal. Chem.* **2020**, *92* (5), 3722−3727.

(14) Cheng, C.; Zhang, R.; Wang, J.; Zhang, Y.; Xiong, S.; Huang, Y.; Yang, M. Porphyrinic Metal−Organic Framework Nanorod-Based

Dual-Modal Nanoprobe for Sensing and Bioimaging of Phosphate. *ACS Applied Materials & Interfaces* **2020**, *12* (23), 26391−26398.
(15) Phouthavong, V.; Manakasettharn, S.; Viboonratanasri, D.; Buajarern, S.; Prompinit, P.; Sereenonchai, K. Colorimetric determination of trace orthophosphate in water by using C18-functionalized silica coated magnetite. *Scientific Reports* **2021**, *11* (1), No. 23073.
(16) Pinyorospathum, C.; Rattanarat, P.; Chaiyo, S.; Siangproh, W.; Chailapakul, O. Colorimetric sensor for determination of phosphate ions using anti-aggregation of 2-mercaptoethanesulfonate-modified silver nanoplates and europium ions. *Sensors and Actuators B: Chemical* **2019**, *290*, 226−232.
(17) Patel, V.; Kruse, P.; Selvaganapathy, P. R. Review—Solid State Sensors for Phosphate Detection in Environmental and Medical Diagnostics. *Journal of The Electrochemical Society* **2022**, *169* (7), No. 077505.
(18) Sari, S. R.; Tsushida, M.; Sato, T.; Tominaga, M. Highly sensitive detection of phosphate using well-ordered crystalline cobalt oxide nanoparticles supported by multi-walled carbon nanotubes. *Materials Advances* **2022**, *3* (4), 2018−2025.
(19) Han, M.; Zhang, W.; Lu, L.; Ma, S.; Feng, S. Enhanced Ultrasensitive Photoelectrochemical Probe for Phosphate Detection in Water Based on a Zirconium−Porphyrin Framework. *ACS Applied Materials & Interfaces* **2022**, *14* (24), 28280−28288.
(20) Naghdi, S.; Cherevan, A.; Giesriegl, A.; Guillet-Nicolas, R.; Biswas, S.; Gupta, T.; Wang, J.; Haunold, T.; Bayer, B. C.; Rupprechter, G.; et al. Selective ligand removal to improve accessibility of active sites in hierarchical MOFs for heterogeneous photocatalysis. *Nat. Commun.* **2022**, *13* (1), 282.
(21) del Castillo-Velilla, I.; Sousaraei, A.; Romero-Muñiz, I.; Castillo-Blas, C.; S. J. Méndez, A.; Oropeza, F. E.; de la Peña O'Shea, V. A.; Cabanillas-González, J.; Mavrandonakis, A.; Platero-Prats, A. E. Synergistic binding sites in a metal-organic framework for the optical sensing of nitrogen dioxide. *Nat. Commun.* **2023**, *14* (1), 2506.
(22) Peng, Y.; Huang, H.; Zhang, Y.; Kang, C.; Chen, S.; Song, L.; Liu, D.; Zhong, C. A versatile MOF-based trap for heavy metal ion capture and dispersion. *Nat. Commun.* **2018**, *9* (1), 187.
(23) Yan, Z.; Liu, X.; Ding, B.; Yu, J.; Si, Y. Interfacial engineered superelastic metal-organic framework aerogels with van-der-Waals barrier channels for nerve agents decomposition. *Nat. Commun.* **2023**, *14* (1), 2116.
(24) Jabbour, C. R.; Parker, L. A.; Hutter, E. M.; Weckhuysen, B. M. Chemical targets to deactivate biological and chemical toxins using surfaces and fabrics. *Nature Reviews Chemistry* **2021**, *5* (6), 370−387.
(25) Winarta, J.; Shan, B.; McIntyre, S. M.; Ye, L.; Wang, C.; Liu, J.; Mu, B. A Decade of UiO-66 Research: A Historic Review of Dynamic Structure, Synthesis Mechanisms, and Characterization Techniques of an Archetypal Metal−Organic Framework. *Crystal Growth & Design* **2020**, *20* (2), 1347−1362.
(26) Pamei, M.; Puzari, A. Luminescent transition metal−organic frameworks: An emerging sensor for detecting biologically essential metal ions. *Nano-Structures & Nano-Objects* **2019**, *19*, No. 100364.
(27) Tian, J.; Liu, Q.; Shi, J.; Hu, J.; Asiri, A. M.; Sun, X.; He, Y. Rapid, sensitive, and selective fluorescent DNA detection using iron-based metal−organic framework nanorods: Synergies of the metal center and organic linker. *Biosensors and Bioelectronics* **2015**, *71*, 1−6.
(28) Cui, Y.; Song, R.; Yu, J.; Liu, M.; Wang, Z.; Wu, C.; Yang, Y.; Wang, Z.; Chen, B.; Qian, G. Dual-Emitting MOF⊃Dye Composite for Ratiometric Temperature Sensing. *Adv. Mater.* **2015**, *27* (8), 1420−1425.
(29) Hao, J.-N.; Yan, B. A water-stable lanthanide-functionalized MOF as a highly selective and sensitive fluorescent probe for Cd2+. *Chemical Communications* **2015**, *51* (36), 7737−7740.
(30) Li, L.; Chen, Q.; Niu, Z.; Zhou, X.; Yang, T.; Huang, W. Lanthanide metal−organic frameworks assembled from a fluorene-based ligand: selective sensing of Pb2+ and Fe3+ ions. *Journal of Materials Chemistry C* **2016**, *4* (9), 1900−1905.
(31) Li, H.-Y.; Wei, Y.-L.; Dong, X.-Y.; Zang, S.-Q.; Mak, T. C. W. Novel Tb-MOF Embedded with Viologen Species for Multi-Photofunctionality: Photochromism, Photomodulated Fluorescence, and Luminescent pH Sensing. *Chem. Mater.* **2015**, *27* (4), 1327−1331.
(32) Abdelhamid, H. N.; Wilk-Kozubek, M.; El-Zohry, A. M.; Bermejo Gómez, A.; Valiente, A.; Martín-Matute, B.; Mudring, A.-V.; Zou, X. Luminescence properties of a family of lanthanide metal-organic frameworks. *Microporous Mesoporous Mater.* **2019**, *279*, 400−406.
(33) Hendrickx, K.; Joos, J. J.; De Vos, A.; Poelman, D.; Smet, P. F.; Van Speybroeck, V.; Van Der Voort, P.; Lejaeghere, K. Exploring Lanthanide Doping in UiO-66: A Combined Experimental and Computational Study of the Electronic Structure. *Inorganic Chemistry* **2018**, *57* (9), 5463−5474.
(34) Islamoglu, T.; Atilgan, A.; Moon, S.-Y.; Peterson, G. W.; DeCoste, J. B.; Hall, M.; Hupp, J. T.; Farha, O. K. Cerium(IV) vs Zirconium(IV) Based Metal−Organic Frameworks for Detoxification of a Nerve Agent. *Chem. Mater.* **2017**, *29* (7), 2672−2675.
(35) Chen, W.; Kitamura, Y.; Zhou, J.-M.; Sumaoka, J.; Komiyama, M. Site-Selective DNA Hydrolysis by Combining Ce(IV)/EDTA with Monophosphate-Bearing Oligonucleotides and Enzymatic Ligation of the Scission Fragments. *J. Am. Chem. Soc.* **2004**, *126* (33), 10285−10291.
(36) Shigekawa, H.; Ishida, M.; Miyake, K.; Shioda, R.; Iijima, Y.; Imai, T.; Takahashi, H.; Sumaoka, J.; Komiyama, M. Extended x-ray absorption fine structure study on the cerium(IV)-induced DNA hydrolysis: Implication to the roles of 4f orbitals in the catalysis. *Appl. Phys. Lett.* **1999**, *74* (3), 460−462.
(37) Tan, K.; Pandey, H.; Wang, H.; Velasco, E.; Wang, K.-Y.; Zhou, H.-C.; Li, J.; Thonhauser, T. Defect Termination in the UiO-66 Family of Metal−Organic Frameworks: The Role of Water and Modulator. *J. Am. Chem. Soc.* **2021**, *143* (17), 6328−6332.
(38) Taddei, M. When defects turn into virtues: The curious case of zirconium-based metal-organic frameworks. *Coord. Chem. Rev.* **2017**, *343*, 1−24.
(39) Liu, L.; Chen, Z.; Wang, J.; Zhang, D.; Zhu, Y.; Ling, S.; Huang, K.-W.; Belmabkhout, Y.; Adil, K.; Zhang, Y.; Slater, B.; Eddaoudi, M.; Han, Y. Imaging defects and their evolution in a metal−organic framework at sub-unit-cell resolution. *Nature Chemistry* **2019**, *11* (7), 622−628.
(40) Smolders, S.; Struyf, A.; Reinsch, H.; Bueken, B.; Rhauderwiek, T.; Mintrop, L.; Kurz, P.; Stock, N.; De Vos, D. E. A precursor method for the synthesis of new Ce(iv) MOFs with reactive tetracarboxylate linkers. *Chemical Communications* **2018**, *54* (8), 876−879.
(41) Varghese, H. T.; Panicker, C. Y.; Philip, D.; Sreevalsan, K.; Anithakumary, V. IR, Raman and SERS spectra of disodium terephthalate. *Spectrochimica Acta Part A: Molecular and Biomolecular Spectroscopy* **2007**, *68* (3), 817−822.
(42) Hadjiivanov, K. I.; Panayotov, D. A.; Mihaylov, M. Y.; Ivanova, E. Z.; Chakarova, K. K.; Andonova, S. M.; Drenchev, N. L. Power of Infrared and Raman Spectroscopies to Characterize Metal-Organic Frameworks and Investigate Their Interaction with Guest Molecules. *Chemical Reviews* **2021**, *121* (3), 1286−1424.
(43) Cirujano, F. G.; Llabrés i Xamena, F. X. Tuning the Catalytic Properties of UiO-66 Metal−Organic Frameworks: From Lewis to Defect-Induced Brønsted Acidity. *The Journal of Physical Chemistry Letters* **2020**, *11* (12), 4879−4890.
(44) Bakuru, V. R.; Churipard, S. R.; Maradur, S. P.; Kalidindi, S. B. Exploring the Brønsted acidity of UiO-66 (Zr, Ce, Hf) metal−organic frameworks for efficient solketal synthesis from glycerol acetalization. *Dalton Transactions* **2019**, *48* (3), 843−847.
(45) Hassan, M. H.; Andreescu, D.; Andreescu, S. Cerium Oxide Nanoparticles Stabilized within Metal−Organic Frameworks for the Degradation of Nerve Agents. *ACS Applied Nano Materials* **2020**, *3* (4), 3288−3294.
(46) Trickett, C. A.; Gagnon, K. J.; Lee, S.; Gándara, F.; Bürgi, H.-B.; Yaghi, O. M. Definitive Molecular Level Characterization of

https://doi.org/10.1021/acs.inorgchem.3c02318
Inorg. Chem. 2023, 62, 20970−20979

Defects in UiO-66 Crystals. *Angewandte Chemie International Edition* **2015**, *54* (38), 11162−11167.
(47) Zhu, Y.; Zheng, J.; Ye, J.; Cui, Y.; Koh, K.; Kovarik, L.; Camaioni, D. M.; Fulton, J. L.; Truhlar, D. G.; Neurock, M.; et al. Copper-zirconia interfaces in UiO-66 enable selective catalytic hydrogenation of CO2 to methanol. *Nat. Commun.* **2020**, *11* (1), 5849.
(48) Shearer, G. C.; Chavan, S.; Bordiga, S.; Svelle, S.; Olsbye, U.; Lillerud, K. P. Defect Engineering: Tuning the Porosity and Composition of the Metal−Organic Framework UiO-66 via Modulated Synthesis. *Chem. Mater.* **2016**, *28* (11), 3749−3761.
(49) Shearer, G. C.; Chavan, S.; Ethiraj, J.; Vitillo, J. G.; Svelle, S.; Olsbye, U.; Lamberti, C.; Bordiga, S.; Lillerud, K. P. Tuned to Perfection: Ironing Out the Defects in Metal−Organic Framework UiO-66. *Chem. Mater.* **2014**, *26* (14), 4068−4071.
(50) Klet, R. C.; Liu, Y.; Wang, T. C.; Hupp, J. T.; Farha, O. K. Evaluation of Brønsted acidity and proton topology in Zr- and Hf-based metal−organic frameworks using potentiometric acid−base titration. *Journal of Materials Chemistry A* **2016**, *4* (4), 1479−1485.
(51) Redfern, L. R.; Ducamp, M.; Wasson, M. C.; Robison, L.; Son, F. A.; Coudert, F.-X.; Farha, O. K. Isolating the Role of the Node-Linker Bond in the Compression of UiO-66 Metal−Organic Frameworks. *Chem. Mater.* **2020**, *32* (13), 5864−5871.
(52) Sun, D.; Fu, Y.; Liu, W.; Ye, L.; Wang, D.; Yang, L.; Fu, X.; Li, Z. Studies on Photocatalytic CO2 Reduction over NH2-Uio-66(Zr) and Its Derivatives: Towards a Better Understanding of Photocatalysis on Metal−Organic Frameworks. *Chem. - Eur. J.* **2013**, *19* (42), 14279−14285.
(53) De Vos, A.; Hendrickx, K.; Van Der Voort, P.; Van Speybroeck, V.; Lejaeghere, K. Missing Linkers: An Alternative Pathway to UiO-66 Electronic Structure Engineering. *Chem. Mater.* **2017**, *29* (7), 3006−3019.
(54) Nasalevich, M. A.; Hendon, C. H.; Santaclara, J. G.; Svane, K.; van der Linden, B.; Veber, S. L.; Fedin, M. V.; Houtepen, A. J.; van der Veen, M. A.; Kapteijn, F.; et al. Electronic origins of photocatalytic activity in d0 metal organic frameworks. *Sci. Rep.* **2016**, *6* (1), No. 23676.
(55) Wu, X.-P.; Truhlar, D. G. Photo-induced Charge Separation and Photoredox Catalysis in Cerium-Based Metal−Organic Frameworks. *ACS Symp. Ser.* **2019**, *1331*, 309−326.
(56) Hassan, M. H.; Soliman, A. B.; Elmehelmey, W. A.; Abugable, A. A.; Karakalos, S. G.; Elbahri, M.; Hassanien, A.; Alkordi, M. H. A Ni-loaded, metal−organic framework−graphene composite as a precursor for in situ electrochemical deposition of a highly active and durable water oxidation nanocatalyst. *Chemical Communications* **2019**, *55* (1), 31−34.
(57) Yuan, S.; Qin, J.-S.; Lollar, C. T.; Zhou, H.-C. Stable Metal−Organic Frameworks with Group 4 Metals: Current Status and Trends. *ACS Central Science* **2018**, *4* (4), 440−450.
(58) Musho, T.; Li, J.; Wu, N. Band gap modulation of functionalized metal−organic frameworks. *Phys. Chem. Chem. Phys.* **2014**, *16* (43), 23646−23653.
(59) Wojciechowski, P. M.; Zierkiewicz, W.; Michalska, D.; Hobza, P. Electronic structures, vibrational spectra, and revised assignment of aniline and its radical cation: Theoretical study. *The Journal of Chemical Physics* **2003**, *118* (24), 10900−10911.
(60) Karimova, N. V.; Luo, M.; Grassian, V. H.; Gerber, R. B. Absorption spectra of benzoic acid in water at different pH and in the presence of salts: insights from the integration of experimental data and theoretical cluster models. *Phys. Chem. Chem. Phys.* **2020**, *22* (9), 5046−5056.
(61) Bůžek, D.; Demel, J.; Lang, K. Zirconium Metal−Organic Framework UiO-66: Stability in an Aqueous Environment and Its Relevance for Organophosphate Degradation. *Inorganic Chemistry* **2018**, *57* (22), 14290−14297.
(62) Rogge, S. M. J.; Yot, P. G.; Jacobsen, J.; Muniz-Miranda, F.; Vandenbrande, S.; Gosch, J.; Ortiz, V.; Collings, I. E.; Devautour-Vinot, S.; Maurin, G.; Stock, N.; Van Speybroeck, V. Charting the Metal-Dependent High-Pressure Stability of Bimetallic UiO-66 Materials. *ACS Materials Letters* **2020**, *2* (4), 438−445.
(63) Wang, L.; Wen, X.; Li, J.; Zeng, P.; Song, Y.; Yu, H. Roles of defects and linker exchange in phosphate adsorption on UiO-66 type metal organic frameworks: Influence of phosphate concentration. *Chemical Engineering Journal* **2021**, *405*, No. 126681.
(64) Xiong, J.; Wang, L.; Qin, X.; Yu, J. Acid-promoted synthesis of defected UiO-66-NH2 for rapid detoxification of chemical warfare agent simulant. *Mater. Lett.* **2021**, *302*, No. 130427.
(65) Hu, Z.; Nalaparaju, A.; Peng, Y.; Jiang, J.; Zhao, D. Modulated Hydrothermal Synthesis of UiO-66(Hf)-Type Metal−Organic Frameworks for Optimal Carbon Dioxide Separation. *Inorganic Chemistry* **2016**, *55* (3), 1134−1141.
(66) Dai, S.; Montero-Lanzuela, E.; Tissot, A.; Baldoví, H. G.; García, H.; Navalón, S.; Serre, C. Room temperature design of Ce(iv)-MOFs: from photocatalytic HER and OER to overall water splitting under simulated sunlight irradiation. *Chemical Science* **2023**, *14* (13), 3451−3461.

https://doi.org/10.1021/acs.inorgchem.3c02318
Inorg. Chem. 2023, 62, 20970−20979